Efficient sensitivity and variability analysis of nonlinear microwave stages through concurrent TCAD and EM modeling

A Test Procedure to Evaluate Magnets Thermal Time Constant of Permanent Magnet Machines

Eric Armando
Dipartimento Energia "G.Ferraris"
Politecnico di Torino
Torino, Italy
eric.armando@polito.it

Aldo Boglietti
Dipartimento Energia "G.Ferraris"
Politecnico di Torino
Torino, Italy
aldo.boglietti@polito.it

Salvatore Musumeci
Dipartimento Energia "G.Ferraris"
Politecnico di Torino
Torino, Italy
salvatore.musumeci@polito.it

Sandro Rubino
Dipartimento Energia "G.Ferraris"
Politecnico di Torino
Torino, Italy
sandro.rubino@polito.it

Enrico Carpaneto
Dipartimento Energia "G.Ferraris"
Politecnico di Torino
Torino, Italy
enrico.carpaneto@polito.it

Daniele Martinello
Dipartimento Energia "G.Ferraris"
Politecnico di Torino
Torino, Italy
daniele.martinello@polito.it

***Abstract*—Thanks to their high torque density, permanent magnet synchronous motors (PMSMs) currently represent the most competitive solution in the electrification processes involving transports and energy production. However, it is known how the torque production of PMSMs is strictly related to the temperature of the permanent magnets (PMs) since the latter affects control performance and efficiency. This issue thus makes necessary the thermal analysis of the machine under consideration. In this scenario, the determination of the PM's thermal time constant covers a pivotal role in implementing an accurate thermal model of PMSMs. Therefore, this paper aims at proposing an experimental test procedure to evaluate the PM's thermal time constant of PMSMs. The proposed procedure can be applied to any PMSM type without being affected by factors such as rotor lamination, shaft, and PM distribution. In this way, accurate and reliable results are obtained. The experimental validation has been carried out on four PMSMs, with different rotor structures, sizes, power, and voltage/current levels. Experimental results demonstrate the validity of the proposed method.**

Keywords—permanent magnet synchronous motors, thermal analysis, thermal time constant, transportation electrification.

I. Introduction

In recent years, significant development has concerned the electric solutions for transports and energy production from renewable [1]. Modern applications like electric and hybrid vehicles [2], [3], more electric aircraft, and railway traction require electric motors with a high torque density and a strong overload capability. Therefore, following the market's needs, the conventional induction machines (IMs) have been progressively replaced with the more performant permanent magnet synchronous motors (PMSMs), increasing efficiency and reducing weight and volume [4].

However, compared to the IMs, the torque production of the PMSMs is significantly affected by the temperature of the permanent magnet (PM), whose effect is to reduce the PM flux density [5]. Consequently, the torque production is compromised [6], making it necessary to increase the current injected in the machine to compensate for the PM flux drop. However, this action reduces the PMSM efficiency and leads to higher Joule losses with consequent thermal stress. Besides, the presented issue gets worse in the case of machine overload, thus requiring accurate thermal modeling [7], [8].

The thermal model of the PMSM allows for understanding several aspects, such as the evaluation of the limits in terms of injected stator currents, avoiding excessive PM overheating. Indeed, the magnetic proprieties of the PM are thermal-sensitive under two aspects [5]. The first is related to the before-mentioned reduction of the PM flux density, although this effect is reversible. Indeed, in the case of PM cooling, the initial magnetic properties are restored fully. Conversely, the second aspect is related to the non-reversible PM demagnetization caused by excessive PM heating. Both aspects get worse in the case of PMSM using fractional-slot windings, thus characterized by a high harmonic content on the magneto-motive force of the air gap [9]. In this case, the harmonic fields induce parasitic currents on the PM surface, increasing losses and PM temperature.

Therefore, most modern electric drives for PMSMs often use two kinds of thermal feedback for implementing proper overload strategies. The first feedback consists of temperature measurements provided by the thermal sensors embedded with the machine (e.g., thermocouples). The second feedback is instead provided by a machine thermal model [7], [10], [11] implemented in parallel with the motor control algorithm. However, both feedback types are often focused on the measured/estimated temperature of the stator winding since the latter represents the most critical part of the machine. Indeed, the thermal sensors are usually placed on the stator winding surface, thus neglecting the thermal effects on the rotor. Concerning the machine's thermal models, they usually consist of first- or second-order equation systems that are focused on the evaluation of the average temperature of the stator winding [12]–[14].

The literature reports several methods to estimate the PM temperature in PMSMs, among which injections of high-frequency signals [15], [16], use of low-cost Hall sensors [17], or implementation of neural networks [18]. An empirical method to evaluate the PM temperature distribution using the harmonic content of the PM-induced back-emf is reported in [19]. Other methods proposed in the literature concern estimating machine magnetization [20] since it depends on the PM temperature, and it may also significantly impact the machine losses [21].

Alternatively, a simple way to monitor the PM temperature consists of estimating the PM flux density, i.e., the machine flux linkage due to the PM presence only. Indeed, the PM flux density and the consequent PM-induced back-emf are proportional to the PM temperature. In this research context, several contributions are reported in the literature. For example, [22], [23] propose estimating the PM flux density using an extended Kalman filter. In [24], the implementation of a neural network is proposed. Instead, a simple approach is presented in [25], where the PM-induced back-emf is sensed in zero current conditions, allowing the estimation of either PM flux density and the PM overtemperature with respect to the rated cold thermal conditions.

Although the techniques mentioned above are different from each other, they can be considered direct methods to

estimate or monitor the PM temperature. However, the literature also reports indirect methodologies that propose the implementation of thermal models [10], [11], [26]. Thus, considering all the machine design data (e.g., materials' proprieties, geometric dimensions of PM and air-gap).

Both direct and indirect methods present advantages and disadvantages. The direct methods are not affected by design factors such as rotor lamination and PM distribution. However, they often require the online measurement of the PM-induced back-emf or the implementation of complex algorithms. On the other hand, the implementation of thermal models requires estimating the Joule- and iron losses, i.e., the conventional measurements of stator currents and mechanical speed (electrical frequency). Also, machine design data must be known, although these are often not available in practice.

According to the presented state-of-art, this paper aims at combining the advantages of direct and indirect methods by evaluating the PM's thermal time constant experimentally. In detail, the proposed procedure is based on the measurements of the PM-induced back-emf, avoiding the need for other motor losses [27], [28] that hinder the evaluation of PM's thermal parameters with high accuracy. In the proposed procedure, the PM-induced back-emf is measured using a calibrated data recorder. Thus, estimating the PM's thermal-time constant with high accuracy. In this way, a robust machine thermal model may be implemented, representing a potential application of the proposed procedure, especially in PMSM motor drives. Indeed, considering the machine control, the knowledge of the PM temperature with an adequate level of confidence allows performing proper overload strategies and improves the torque regulation's performance.

According to the authors' best knowledge, this paper represents one of the first attempts to evaluate the PM's thermal time constant experimentally. Therefore, the contributions of the proposed test procedure to the existing literature can be summarized as follows:

1) Accurate evaluation of the PM's thermal time constant of any PMSM, regardless of the PM distribution inside the rotor lamination.
2) Simultaneous monitoring of the stator winding temperature and PM flux density during the thermal transients, allowing the correlation between them.

The experimental validation of the proposed measurement technique has been carried out on four PMSMs that present a different PM distribution on the rotor. This paper builds on [29], [30] and brings in added value by including:

1) Experimental validation on further PMSMs having a surface-mount PM distribution.
2) Evaluation of the derating that affects the torque production of the PMSMs after the PM heating.
3) Further considerations related to the impact of PM heating on machine efficiency.
4) Comparative evaluation between the PM's thermal time constant obtained through the proposed test procedure and the one computed theoretically using the machine design data.

The paper is organized as follows. The proposed measurement technique is described in Section II. The computation method of the PM's thermal time constant is reported in Section III. The test rig to perform the proposed test procedure is described in Section IV. Experimental validation is provided in Section V, while the theoretical confirmation using the machines' design data is reported in Section VI. Further remarks are reported in Section VII. Lastly, Section VIII reports paper conclusions.

II. Measurement technique

The proposed test procedure performs the heating of the motor under test (MUT) to monitor the increment of the stator winding resistance R_s and the decay of the PM flux linkage λ_m. The first is related to the average temperature of the stator winding T_s, while the decay of the PM flux linkage is representative of the PM's average temperature. After performing the heating procedure, the stator winding temperature should be equal to the rated one. Therefore, the time duration of the heating procedure can be a few minutes up to several hours, according to the machine dimensions, i.e., its thermal time constant.

A. Electromagnetic model of a PMSM

To facilitate the understanding of the proposed test procedure, the electromagnetic model of a generic PMSM in rotating (dq) coordinates is summarized as follows [31]:

$$\begin{cases} v_d = R_s \cdot i_d + L_d \cdot \dfrac{d}{dt} i_d - p \cdot \omega_m \cdot L_q \cdot i_q \\ v_q = R_s \cdot i_q + L_q \cdot \dfrac{d}{dt} i_q + p \cdot \omega_m \cdot \left(L_d \cdot i_d + \lambda_m \right) \end{cases} \quad (1)$$

where (v_d,v_q), (i_d,i_q), and (L_d,L_q) are the (dq) values of phase voltages, phase currents, and inductances, respectively. The rotor mechanical speed is denoted with ω_m while p stands for the machine pole pairs. According to (1), the steady-state (dq) quantities (uppercase characters) are computed as follows:

$$\begin{cases} V_d = R_s \cdot I_d - p \cdot \omega_m \cdot L_q \cdot I_q \\ V_q = R_s \cdot I_q + p \cdot \omega_m \cdot \left(L_d \cdot I_d + \lambda_m \right) \end{cases} \quad (2)$$

B. Test procedure

During the test procedure, the time evolutions of the stator winding resistance and PM flux linkage are acquired with a proper time-resolution Δt. According to the usual time-duration of the thermal transients involving the electrical machines [7], [32], a good compromise consists of evaluating both variables with a time-resolution of 1-3 minutes. Consequently, the heating procedure consists of a sequence of a predefined number n of thermal points.

In each thermal point, three actions are performed as follows: *i*) MUT heating, *ii*) identification of the stator resistance followed by *iii)* identification of the PM flux linkage. An application example is presented, facilitating the understanding. A machine having an overall thermal time constant of 60 minutes is considered. Therefore, for reaching the steady-state thermal conditions, the time-duration of the heating procedure should be at least five times the value of the thermal time constant, corresponding to 300 minutes. Consequently, assuming that time evolutions of the stator winding resistance and PM flux linkage must have a time-resolution of 3 minutes (Δt), the resulting number of thermal points composing the heating procedure is n = 100 (300/3).

In each thermal point, the heating action is performed by injecting a predefined combination of (dq) currents in the MUT, using a conventional field-oriented control (FOC) scheme [31]. The amplitude of the current vector $I_{th,pk}$ should be set for injecting the RMS thermal current $I_{th,rms}$ of the MUT ($I_{th,pk} = \sqrt{2} \cdot I_{th,rms}$). Therefore, this value usually corresponds to the rated current of the machine. Although there are no constraints on distributing the thermal current amplitude on the (dq) axes, the q-axis current component is set at zero. In this way, the torque production of the MUT is avoided. The d-axis current component is conventionally set positive, thus having a flux-intensifying action.

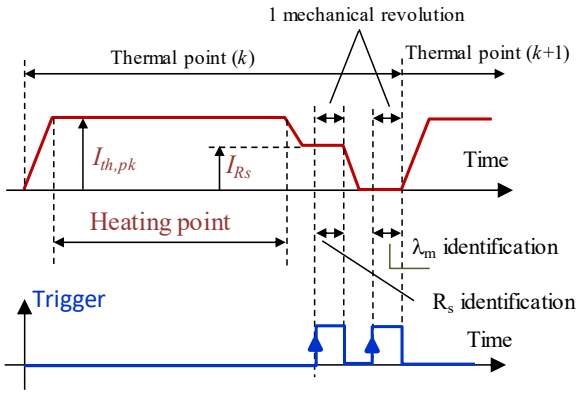

Fig. 1. Profile of the *d*-axis current in a generic thermal point *k* [33].

Therefore, the proposed test procedure consists of actively controlling the *d*-axis current component, leading to the profile shown in Fig. 1. In each thermal point, it is noted that after the MUT heating, the identification of the stator resistance followed by that of the PM flux linkage is performed. Concerning the identification of the stator resistance, the *d*-axis current is set at a predefined target I_{Rs}.

This value should guarantee the proper identification of the stator resistance, avoiding excessive MUT heating. Therefore, it is recommended to set the value of the current reference I_{Rs} lower than the thermal current, as shown in Fig. 1. Each thermal point ends with the identification of the PM flux linkage λ_m. This variable is estimated by sensing the PM-induced back-emf, thus requiring to control both (*dq*) current components at zero (Fig. 1). Since the PM-induced back-emf need to be sensed, the proposed test procedure is performed by rotating the MUT at a constant mechanical speed. Therefore, a driving machine (DM) acting as prime mover must be connected to the MUT rotor. Concerning the machine speed, this value must allow proper back-emf sensing. However, the mechanical speed must be kept low to avoid significant losses on the MUT lamination (stator core).

The flow diagram summarizing the main steps of the proposed test procedure is shown in Fig. 2.

C. *Identification of stator resistance and PM flux linkage*

The measurements of phase currents, line-to-line voltages, and mechanical rotor position are performed for each thermal point. Such quantities are sampled and stored using a calibrated data recorder. According to the pole pairs number *p* of the MUT, the *d*-axis position is computed from the mechanical rotor position. The mounting offset of the mechanical sensor (e.g., resolver or encoder) is compensated using the commissioning procedures usually implemented in electric drives. Once the *d*-axis position is known, the Park transformation on the sampled values of phase-currents and line-to-line voltages is applied [31]. In this way, the (*dq*) components of stator currents (i_d,i_q) and stator voltages (v_d,v_q) are computed.

1) Identification of the stator resistance: The generic thermal point *k* (*k*=1,…,*n*) is considered. The steady-state values of *d*-axis voltage V_d and *d*-axis current I_d are computed as the average of all measurements performed in one mechanical revolution. In this way, the effects of the stator slots are mitigated. In summary, the stator resistance in the generic thermal point *k* (*k* = 1,…,*n*) is computed as:

$$R_s(k) = \frac{V_d(k)}{I_d(k)} \cong \frac{V_d(k)}{I_{R_s}} \tag{3}$$

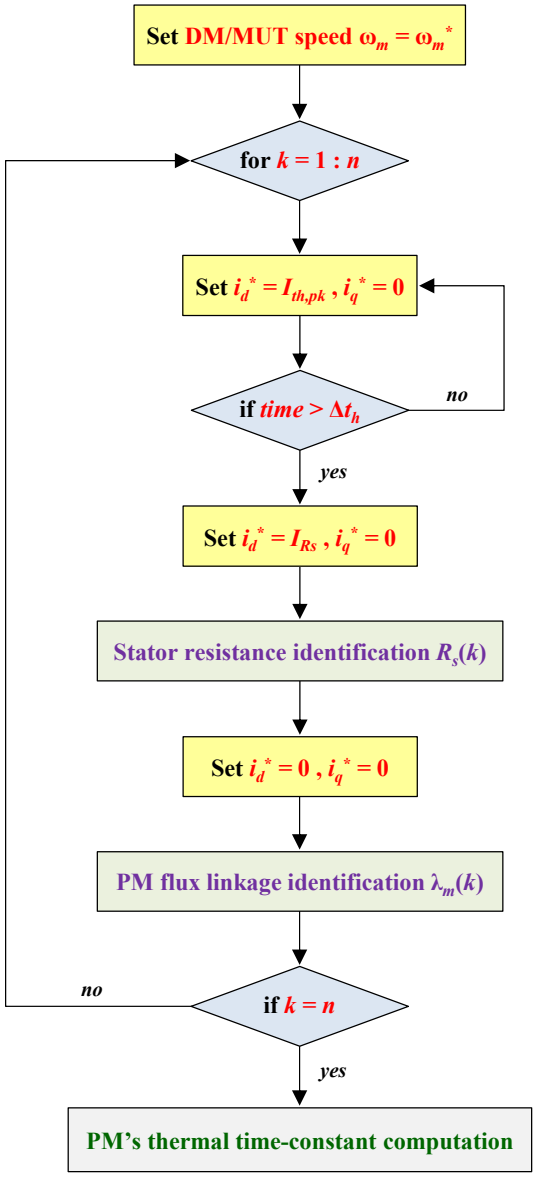

Fig. 2. Flow diagram of the proposed test procedure (Δt_h is the heating time, lower than the time-resolution of thermal point Δt).

The approximation in (3) is valid since the *d*-axis current is closed-loop controlled at the value I_{Rs} using the FOC scheme. The value of stator resistance is then used to evaluate the average temperature of the stator winding as [34]:

$$T_s(k) = \frac{R_s(k)}{R_{s,0}} \cdot \left(K_T + T_{s,0}\right) - K_T \tag{4}$$

where $R_{s,0}$ is the stator winding resistance evaluated at the starting of the heating procedure and related to the initial winding temperature $T_{s,0}$. Finally, K_T is the "characteristic temperature" of the conductive material (K_T = 234.5 °C for copper, K_T = 225 °C for aluminum).

2) Identification of the PM flux linkage: The evaluation of the PM flux linkage is performed by sensing the PM-induced back-emf. Therefore, by imposing the zero-current condition through the FOC scheme, the (*dq*) voltages of the MUT coincide with the PM-induced back-emf. Similarly to the identification of the stator resistance, the variables of interest are computed as the average of all measurements performed in one mechanical revolution, mitigating the effects of the stator slots. Therefore, the PM flux linkage λ_m at the generic thermal point *k* (*k* = 1,…,*n*) is computed as:

$$\lambda_m(k) = \frac{V_q(k)}{p \cdot \Omega_m(k)} \tag{5}$$

where V_q and Ω_m are the average values of q-axis voltage and mechanical speed, respectively. The variables (3)-(5) are so computed in the continuous-time domain as:

$$X(t) = X(k \cdot \Delta t) \qquad X = (R_s, T_s, \lambda_m) \tag{6}$$

According to the presented methodology, the following considerations can be made:

- The proposed test procedure automatically accounts for the PM distribution in the rotor lamination since the PM-induced back-emf is directly sensed. Indeed, as known from the literature, these voltages correspond to the average spatial effect of the PM flux distribution along the airgap. Therefore, it is possible to assume that the decay of the PM flux linkage is directly related to the average PM temperature, thus supporting the proposed methodology.
- Since the evaluation of the PM flux linkage is performed in no-load conditions, the saturation effects usually caused by the stator currents are avoided. Therefore, the machine heating can be performed regardless of the sign of the d-axis current.

Finally, it is further highlighted how the time windows in which the stator resistance and the PM flux linkage are evaluated last just one mechanical revolution. Therefore, assuming a mechanical speed of 100 rpm, the PM flux linkage is evaluated in only 0.6 s. If comparing this time with the 1-3 minutes in which the MUT is heated by injecting the rated current, it can be assumed that the average PM temperature is practically constant in the time window in which the PM flux linkage is evaluated.

III. PM Thermal Time Constant Computation

The experimental results that will be shown in Section V demonstrate how a first-order time-differential model can describe the decay of the PM flux linkage as:

$$\lambda_m(t) = \lambda_{m,\infty} + \left[\lambda_{m,0} - \lambda_{m,\infty}\right] \cdot e^{-t/\tau_m} \tag{7}$$

where τ_m is the PM's thermal time constant while $\lambda_{m,0}$ and $\lambda_{m,\infty}$ are the values of PM flux linkage at the starting and end of the test procedure, respectively. Hence, the value of the PM flux linkage at the procedure end corresponds to the steady-state thermal condition of the MUT. The PM's thermal time constant τ_m is computed using the least-squares method on (7) and the experimental time-evolution (5), (6).

Although it consists of an approximation, also the time-evolutions of the stator winding resistance and stator winding temperature can be described by a first-order time-differential model as:

$$\begin{cases} R_s(t) = R_{s,0} + \left[R_{s,\infty} - R_{s,0}\right] \cdot \left(1 - e^{-t/\tau_s}\right) \\ T_s(t) = T_{s,0} \ + \left[T_{s,\infty} - T_{s,0}\right] \cdot \left(1 - e^{-t/\tau_s}\right) \end{cases} \tag{8}$$

where $R_{s,\infty}$ is the stator winding resistance at the end of the heating procedure, corresponding to the steady-state thermal condition of the MUT windings $T_{s,\infty}$.

Concerning τ_s, it can be considered as an equivalent thermal time constant of the MUT. Therefore, it represents the thermal path between the stator winding and the external environment. The equivalent thermal time constant τ_s is computed by using the method of the least squares on (8) and experimental time-evolutions (3), (4), (6).

IV. Experimental Test Rig

The test bench to evaluate the PM's thermal time constant is shown in Fig. 3, and it corresponds to the experimental setup usually used to identify the magnetic model of synchronous ac motors [33], [35], [36]. As stated in Section III, the MUT is connected to a driving machine (DM) that usually consists of a speed-controlled spindle drive. It is highlighted how the DM's rated power can be meager, as the proposed procedure does not require the torque production of the MUT.

Two possible configurations of the test rig can be adopted. The first one consists of a back-to-back configuration (Fig. 3, top) where the inverters feeding the MUT and DM share the dc bus, i.e., dc-link voltage v_{dc}. Alternatively, a dedicated test rig for the DM (Fig. 3, bottom) can be used. According to the test bench used for the experimental validation, the second configuration is considered, whose layout is shown in Fig. 4. Compared to Fig. 3 and Fig. 4 that show the test rig to identify the flux linkage maps of the MUT, the presence of a torque sensor along the mechanical connection between MUT and DM is not necessary to perform the proposed test procedure. As stated in Section III, the MUT is current-controlled using a FOC scheme [31] implemented on a conventional digital controller that also provides the DM's reference speed.

The proposed measurement system consists of a data recorder that collects the samples of MUT phase currents, MUT line-to-line voltages, and mechanical position (using a resolver or an encoder). The measurements of phase currents and mechanical position are also necessary to implement the FOC algorithm that performs the MUT control (Fig. 4). The direct measurement of the MUT line-to-line voltages is strongly recommended [33]. In this way, the compensation of the voltage errors introduced by the inverter feeding the MUT is avoided [37].

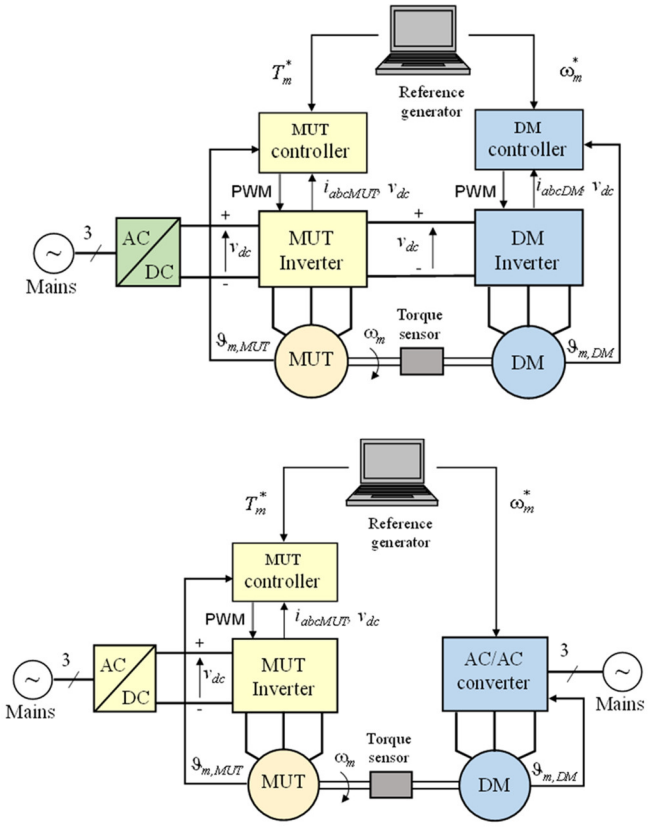

Fig. 3. Test rig for the determination of the PM's thermal time constant: back-to-back configuration (top), dedicated test rig for DM (bottom).

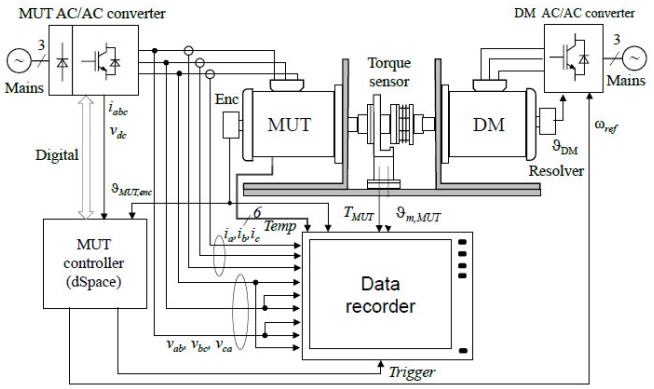

Fig. 4. Layout of the experimental test rig [36].

Therefore, using the proposed measurement system, the line-to-line pulse-width modulation (PWM) voltages of the MUT are directly measured using high-voltage/high-speed acquisition channels [36]. Finally, the time-fundamental components of these voltages are reconstructed by elaborating the sampled data with the software integrated with the data recorder.

V. Experimental Validation

The proposed measurement technique has been experimentally validated on four PMSMs.

The first machine (MUT_1) is a spoke-rotor interior permanent magnet (IPM) motor having 8 poles. The second machine (MUT_2) is a fractional-slot surface-mount permanent magnet (SPM) motor having 36 poles. Finally, the third (MUT_3) and fourth (MUT_4) machines are SPM motors with distributed windings, having 8 and 10 poles, respectively. TABLE I. lists the primary data of the MUTs.

Views of MUT_2 and MUT_4, both considered for the computation of the PM's thermal time constant using the design data, are shown in Fig. 5 and Fig. 6, respectively.

Finally, all the motors used for the experimental validation are air-cooled without the presence of fans (natural convection).

A. Test Setup

The reference speed of the DM has been set at 300 rpm and 100 rpm for MUT_1 and MUT_2, respectively, while 500 rpm for MUT_3 and MUT_4.

A view of the test rig when MUT_4 has been tested is shown in Fig. 7. The mechanical rotor position has been measured with an incremental encoder having a resolution of 3600 pulses/rev for MUT_1 and MUT_2, and 2500 pulses/rev for MUT_3 and MUT_4.

The MUT inverter has consisted of a three-phase insulated gate bipolar transistors (IGBTs) power module. It has been fed by a reversible dc source at 500 V (60 V for testing MUT_3). The switching frequency has been set at 16 kHz, with software implemented dead-time of 1 µs. The digital controller has consisted of the dSPACE® DS1103, while the sampling frequency has been set at 16 kHz (single-edge PWM).

Finally, the data recorder has consisted of Genesis 7tA (Gen7tA) from HBM [38]. It consists of a high-performance transient recorder and calibrated data acquisition system to perform the measurements of line-to-line voltages, phase currents, and mechanical rotor position (Fig. 8). Thanks to its high-voltage/high-speed acquisition channels (voltage card GN610B, 18 bit, 2 MS/s), the Gen7tA allows the direct measurement of the PWM line-to-line voltages.

TABLE I. Primary Data of the Machines Under Test

	MUT_1	MUT_2	MUT_3	MUT_4
Rotor type	IPM Spoke Rotor	SPM Outer Rotor	SPM Internal Rotor	SPM Internal Rotor
Winding type*	C	C	D	D
Poles number	8	36	8	10
Rated power	600 W	800 W	1 kW	2.3 kW
Rated speed	3000 rpm	166 rpm	3000 rpm	4400 rpm
Rated voltage	190 V	220	28	350
Rated current	2.75	5	30	4.4

* C = Concentrated, D = Distributed

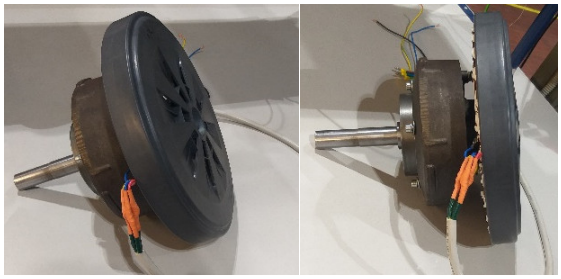

Fig. 5. View of MUT_2 (fractional-slots SPM with outer rotor).

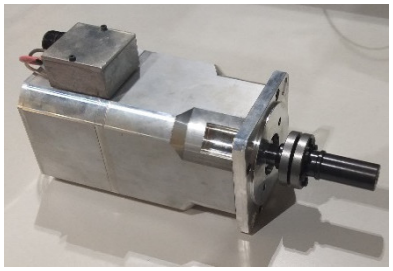

Fig. 6. View of MUT_4 (conventional SPM with internal rotor).

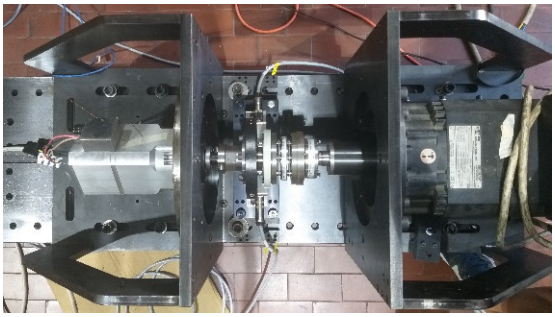

Fig. 7. View of MUT_4 (left) and DM (right).

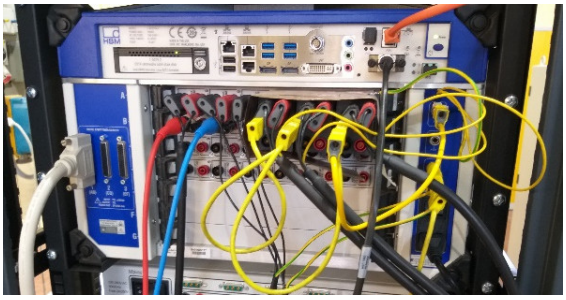

Fig. 8. View of the data recorder Gen7tA from HBM [38].

Finally, using the software integrated with the instrument (HBM Perception), the reconstruction of the time-fundamental voltage components has been performed.

B. Experimental results

In the following, experimental results obtained on the MUTs are presented, thus reporting the computed values of the thermal time constants of PM τ_m and stator winding τ_s.

1) MUT_1: The decay of PM flux linkage and the increment of the stator winding temperature for MUT_1 are shown in Fig. 9 and Fig. 10, respectively. Both PM and stator winding are in steady-state thermal conditions. The steady-state stator winding temperature is near 132.6 °C, while the overall decline of the PM flux linkage is about 24.7 %. Therefore, the PM of MUT_1 shows a significant temperature-dependent behavior. According to (7), (8) the computed values of thermal time constants are τ_m = 48 min and τ_s = 36 min.

2) MUT_2: The decay of PM flux linkage and the increment of the stator winding temperature for MUT_2 are shown in Fig. 11 and Fig. 12, respectively. The steady-state stator winding temperature is near 100.7 °C, while the overall decline of PM flux linkage is about 5.9 %. Therefore, the PM of MUT_2 shows a robust temperature-independent behavior. Regarding the thermal time constants, according to (7), (8), the computed values are τ_m = 44 min and τ_s = 32 min.

3) MUT_3: MUT_3 exhibits a temperature-independent behavior, thus obtaining experimental results similar to those of MUT_2, as shown in Fig. 13 and Fig. 14. The steady-state stator winding temperature is near 69.5 °C, while the overall decline of PM flux linkage is about 3.9 %. The computed values of thermal time constants of PM and stator winding are τ_m = 39 min and τ_s = 38 min, respectively. Finally, it is noted how for MUT_3, the use of a single time constant to represent the time-evolution of the stator winding is an approximation. Indeed, the time constants that characterize the thermal path between the stator winding and the external environment are comparable to each other [8], [13], as confirmed by the small-time duration of the thermal transient, too. Further considerations are not reported here since this paper focuses on evaluating the PM's thermal time constant.

4) MUT_4: The decay of PM flux linkage and the increment of the stator winding temperature for the MUT_4 are shown in Fig. 15 and Fig. 16, respectively. The steady-state stator winding temperature is near 58.9 °C, while the overall decline of the PM flux linkage is about 2.8 %. Although the decay of the PM flux linkage is negligible, it has been measured with high accuracy with the proposed test procedure, thus allowing the computation of the related thermal time constant. Therefore, from Fig. 15, it is noted how the PM of MUT_4 shows a temperature-independent behavior in the rated supply conditions, i.e., injection of the rated current.

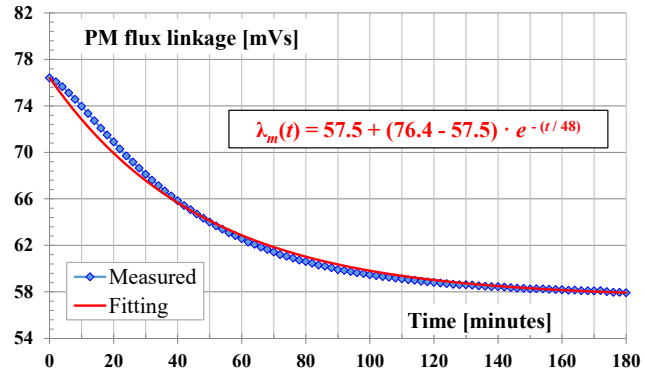

Fig. 9. Decay of the PM flux linkage for MUT_1.

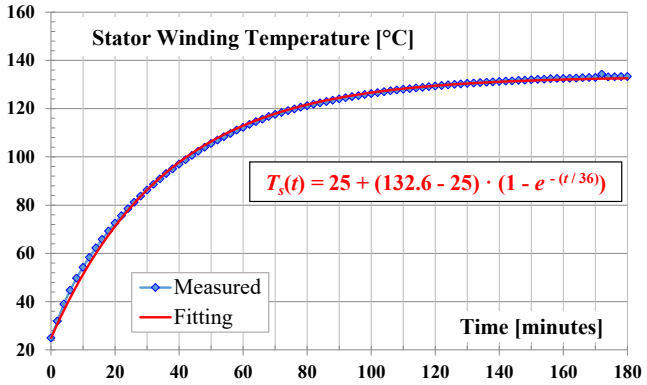

Fig. 10. Increment of the stator winding temperature for MUT_1.

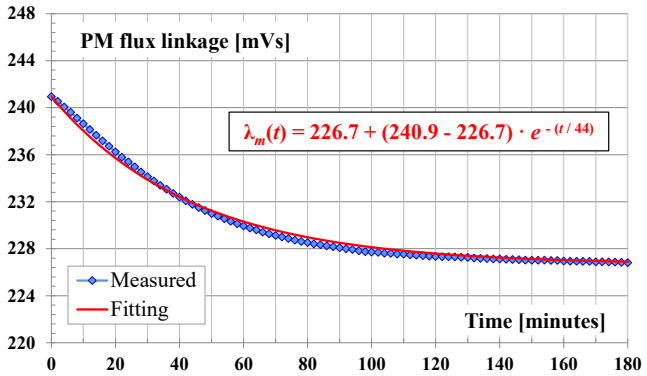

Fig. 11. Decay of the PM flux linkage for MUT_2.

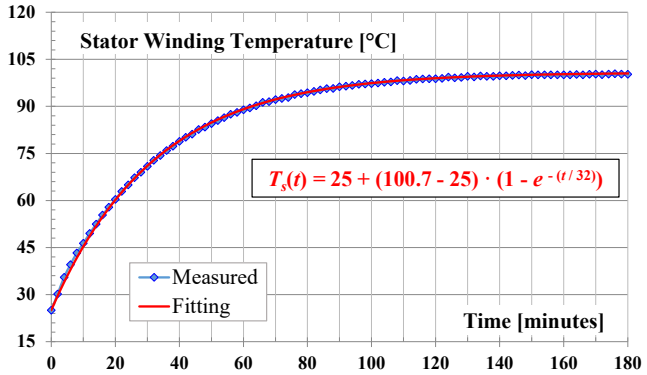

Fig. 12. Increment of the stator winding temperature for MUT_2.

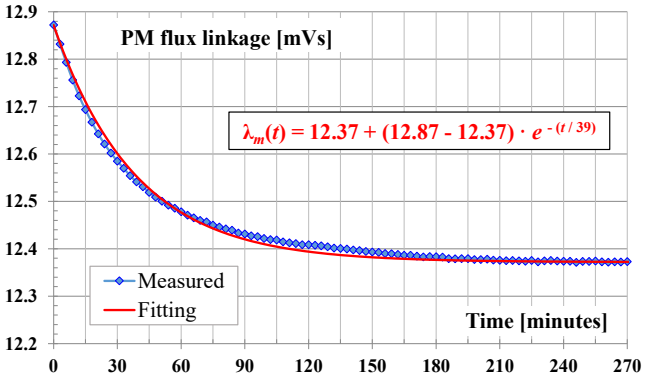

Fig. 13. Decay of the PM flux linkage for MUT_3.

Concerning the thermal time constants of MUT_4, according to (7), (8), the computed values are τ_m = 59 min and τ_s = 44 min.

TABLE II. summarizes the results obtained for the MUTs, together with the main settings of the proposed test procedure in terms of thermal points' number n and their time-length Δt, the latter corresponding to the time-resolution whereby the thermal transients have been identified.

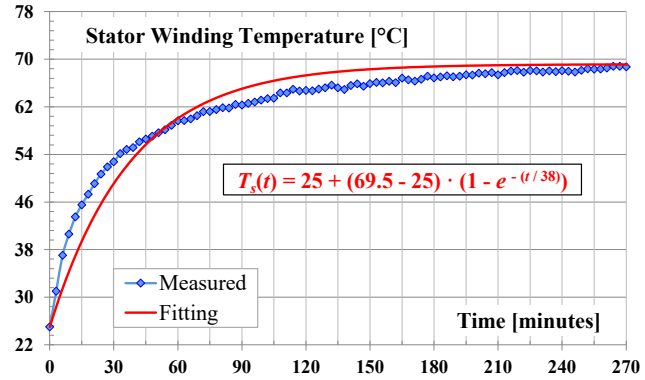

Fig. 14. Increment of the stator winding temperature for MUT_3.

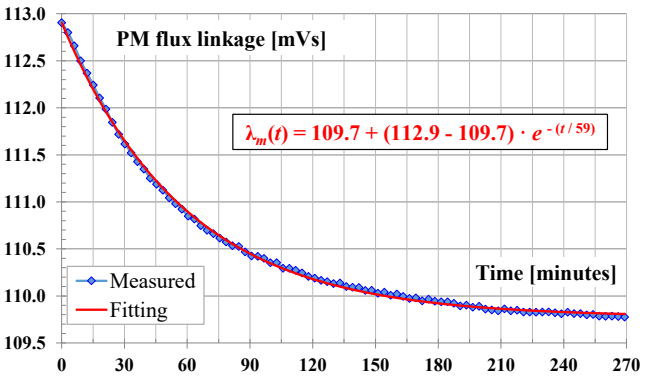

Fig. 15. Decay of the PM flux linkage for MUT_4.

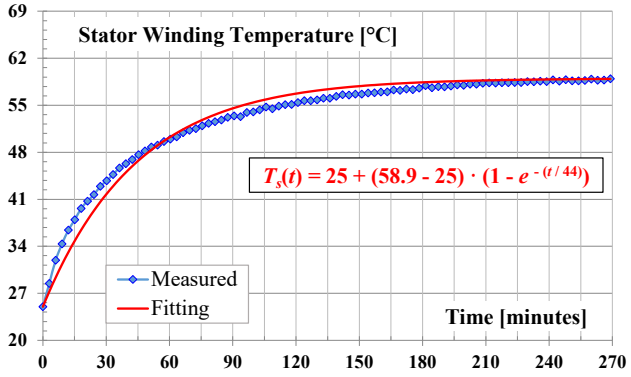

Fig. 16. Increment of the stator winding temperature for MUT_4.

TABLE II. SUMMARY OF THE OBTAINED EXPERIMENTAL RESULTS

	MUT_1	MUT_2	MUT_3	MUT_4
n	90	135	90	90
Δt	2 min	2 min	3 min	3 min
$R_{s,0}$	3.40 Ω	7.40 Ω	26.0 mΩ	1.05 Ω
$R_{s,\infty}$	4.81 Ω	9.56 Ω	30.4 mΩ	1.19 Ω
$T_{s,0}$	25°C	25 °C	25°C	25°C
$T_{s,\infty}$	132.6 °C	100.7 °C	69.5 °C	58.9 °C
τ_s	36 min	32 min	38 min	44 min
$\lambda_{m,0}$	76.4 mVs	240.9 mVs	12.87 mVs	112.9 mVs
$\lambda_{m,\infty}$	57.5 mVs	226.7 mVs	12.37 mVs	109.7 mVs
τ_m	48 min	44 min	39 min	59 min

VI. THEORETICAL VALIDATION

The proposed methodology allows computing the PM's thermal time constant without separating thermal resistance and thermal capacitance contributions. However, for MUT_2 (see Fig. 5) and MUT_4 (see Fig. 6), the machine design data were available, allowing the computation of these parameters. In this way, the PM's thermal time constant has been computed theoretically. Thus, comparing this value with the one obtained experimentally (see TABLE II.), the theoretical validation of the proposed methodology has been carried out.

The computation of the thermal parameters has been performed as follows. The PM is heated due to the stator Joule losses, as schematically shown in Fig. 17. Therefore, the heat flow crosses the air gap before reaching the PM and the rotor lamination. Consequently, the thermal resistance that represents the heat path is composed of the sum of the contributions of *i*) air-gap, *ii*) PM, and *iii*) rotor lamination. However, since the thermal conductivity of the air, i.e., 0.026 W/(m·K), is much higher than the ones of rotor lamination and PM, only the air-gap thermal resistance R_{ag} is considered. According to [39], this parameter is computed as:

$$R_{ag} = \frac{1}{2\pi \cdot k_{air} \cdot L_s} \cdot \ln\left(\frac{r_{is}}{r_{is} - l_{ag}}\right) \tag{9}$$

where r_{is} is the inner stator radius, l_{ag} is the air gap thickness, k_{air} is the thermal conductivity of the air, while L_s is the lamination length. Concerning the thermal capacitances of PM C_{PM} and rotor laminations C_{rl}, both involved in the thermal transients, they are computed as:

$$C_{PM} = c_{PM} \cdot m_{PM} \qquad C_{rl} = c_{rl} \cdot m_{rl} \tag{10}$$

where m_{PM} and m_{rl} are the overall masses of PM and rotor lamination, respectively, both computed using the machine design data. The specific heat capacity of the rotor lamination c_{rl} corresponds to the one of the iron, i.e., 452.2 J/(kg·K). Regarding the specific heat capacity c_{PM} of the PM, it is necessary to consider its magnetic material as [40], [41]:

- c_{PM} = 334.9 J/(kg·K) for hard ferrite;
- c_{PM} = 355.9 J/(kg·K) for Sm-Co;
- c_{PM} = 502.4 J/(kg·K) for NdFeB.

Finally, from the values of thermal resistance and thermal capacitances, the theoretical value of the PM's thermal time constant $\tau_{PM,th}$ is computed as:

$$\tau_{PM,th} \cong R_{ag} \cdot (C_{PM} + C_{rl}) \tag{11}$$

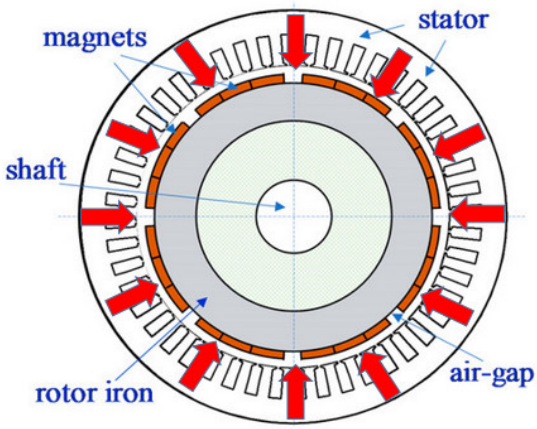

Fig. 17. Heat flow (red arrows) from stator to the rotor in an SPM machine.

TABLE III. COMPUTED THERMAL PARAMETERS AND COMPARISON WITH EXPERIMENTAL DATA

	MUT_2	**MUT_4**
R_{ag}	4.93 K/W	8.68 K/W
C_{PM}	282.1 J/K	94.7 J/K
C_{rl}	223.9 J/K	340.3 J/K
$\tau_{PM,th}$ @ C_{rl} = **0**	23.2 min	13.9 min
$\tau_{PM,th}$	41.5 min	63.6 min
$\tau_{PM,exp}$ (*see* **TABLE II.**)	44 min	59 min

TABLE III. summarizes the results that have been computed for MUT_2 and MUT_4. Also, the comparison between the theoretical and experimental values of PM's thermal time constant is reported. It is noted how without considering the thermal capacitance of the rotor lamination C_{rl} in (11), the theoretical value of the PM's thermal time constant mismatches to the experimental one significantly. However, by applying (11) rigorously, the theoretical and experimental values of PM's thermal time constant slightly differ from each other. In detail, considering the experimental values as the reference ones, differences of 5.7 % for MUT_2 and -7.8 % for MUT_4 are obtained, resulting in both acceptable and so providing the theoretical validation of the proposed test procedure.

VII. ASSESSMENTS ON THE PM TEMPERATURE VARIATION

The time evolutions of the stator winding temperature and PM flux linkage allow performing some assessments. The first one is related to the derating of the torque production caused by the decay of the PM flux linkage. Indeed, according to the FOC theory [31], the torque produced through the PM M_{PM} is computed as:

$$M_{PM} = \frac{3}{2} \cdot p \cdot \lambda_m \cdot i_q \tag{12}$$

Therefore, supposing that MUT is in steady-state thermal conditions and isothermal with the external environment (T_s=$T_{s,0}$), the injection of the rated MUT's current I_n (RMS) leads to the decay of the PM flux linkage as in (7). Although the proposed identification procedure injects the rated current along the *d*-axis, such a current is distributed on both (*dq*) axes to maximize the torque production in a real application.

Since this paper focuses on the thermal behavior of the PM, it is supposed that the MUT current is injected only on the *q*-axis, thus maximizing the torque produced through the PM. Consequently, considering a continuative duty (S1) of the drive [42], the time evolution of the torque produced through the PM is:

$$M_{PM}(t) = M_{PM,\infty} + \left[M_{PM,0} - M_{PM,\infty} \right] \cdot e^{-t/\tau_m} \tag{13}$$

where the initial $M_{PM,0}$ and steady-state $M_{PM,\infty}$ torques are computed as:

$$\begin{aligned} M_{PM,0} &= \sqrt{2} \cdot \frac{3}{2} \cdot p \cdot \lambda_{m,0} \cdot I_n \\ M_{PM,\infty} &= \sqrt{2} \cdot \frac{3}{2} \cdot p \cdot \lambda_{m,\infty} \cdot I_n \end{aligned} \tag{14}$$

It is noted how the torque produced in steady-steady state thermal conditions depends on the decay of the PM flux linkage as:

$$k_M = \frac{M_{PM,\infty}}{M_{PM,0}} = \frac{\lambda_{m,\infty}}{\lambda_{m,0}} \tag{15}$$

where k_M stands for the derating factor of the torque production related to the PM heating.

Therefore, thanks to the proposed test procedure, the evaluation of this parameter can be performed, as demonstrated in (15). However, the derating of the MUT performance can also be evaluated in terms of efficiency. Indeed, considering that the MUT operates at the rated speed $\omega_{m,n}$, the mechanical power P_{out} is computed as:

$$P_{out}(t) = M_{PM}(t) \cdot \omega_{m,n} \tag{16}$$

Concerning the input power of the MUT P_{in}, by neglecting the iron and mechanical losses, this is computed as:

$$P_{in}(t) = P_{out}(t) + P_J(t) \tag{17}$$

where according to (8), the Joule losses P_J are computed as:

$$P_J(t) = P_{J,0} + \left[P_{J,\infty} - P_{J,0} \right] \cdot \left(1 - e^{-t/\tau_s} \right) \tag{18}$$

It is noted how the Joule losses depend on the initial and steady-state values of the stator resistance as:

$$\begin{aligned} P_{J,0} &= 3 \cdot R_{s,0} \cdot I_n^2 \\ P_{J,\infty} &= 3 \cdot R_{s,\infty} \cdot I_n^2 \end{aligned} \tag{19}$$

Finally, the MUT's efficiency is computed as:

$$\eta(t) = \frac{P_{out}(t)}{P_{in}(t)} \tag{20}$$

Therefore, the derating factor of the MUT's efficiency related to the PM heating $k\eta$ can be computed as:

$$k_\eta = \frac{\eta_\infty}{\eta_0} = \frac{\eta(t \to \infty)}{\eta(t=0)} \tag{21}$$

where η_0 and η_∞ are the initial and steady-state efficiency values. The results of the above-presented analysis on the MUTs are shown in the following.

1) MUT_1: According to the experimental results obtained on MUT_1 (see Fig. 9 and Fig. 10), the decay of the PM flux linkage leads to a significant derating of the PM torque, as shown in Fig. 18. It is noted how using (13), (15), the torque derating factor is near to k_M = 0.753, corresponding to a drop of the PM torque of about 24.7 %. Concerning the evolutions of the input and output MUT powers in rated operating conditions, together with the related efficiency, the expected results are shown in Fig. 19. It is noted how, supposing to inject the rated current of MUT to produce the PM torque, the increment of the stator winding temperature, and the simultaneous decay of the PM flux linkage, lead to a reduction of the MUT's efficiency near to 10 %. Indeed, the expected MUT's efficiency starts from a value of η = 0.88 up to reduce itself at a value near to η = 0.79 in steady-state thermal conditions, i.e., $k\eta$ = 0.898.

2) MUT_2: Compared to MUT_1, the decay of the PM flux linkage of MUT_2 is more reduced (see Fig. 11), further confirmed by the derating of the PM torque shown in Fig. 20. In this case, the torque derating factor is about k_M = 0.941, corresponding to a PM torque drop of 5.9 %. Concerning the evolutions of the MUT's input- and output- powers in rated operating conditions, together with the efficiency, the expected results are shown in Fig. 21. It is noted how the MUT's efficiency starts from a value of η = 0.59 and decreases to η = 0.51 in steady-state thermal conditions, corresponding to a derating factor of $k\eta$ = 0.864. In this case, the MUT's efficiency is strongly affected by the high value of the stator resistance (see TABLE II.), whose increment has a higher impact than the decay of the PM flux linkage.

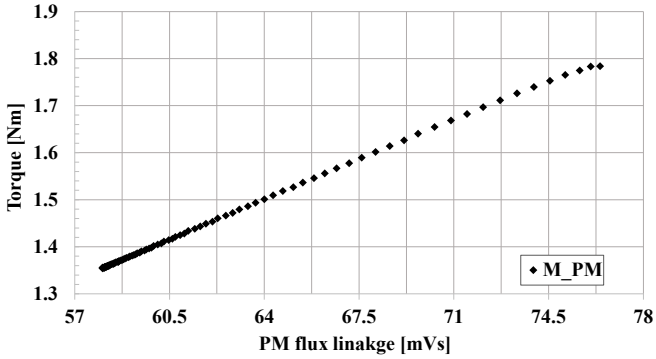

Fig. 18. Derating of the torque production for MUT_1.

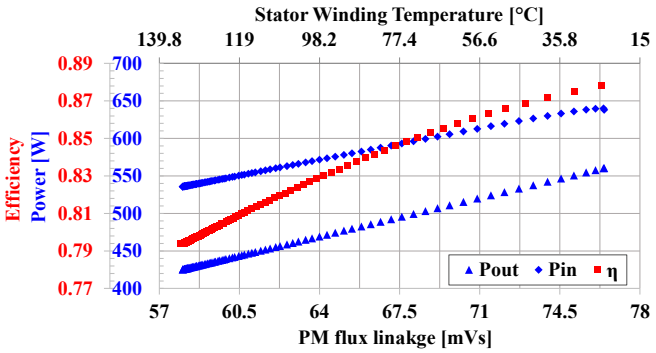

Fig. 19. Expected efficiency of the PM torque production for MUT_1.

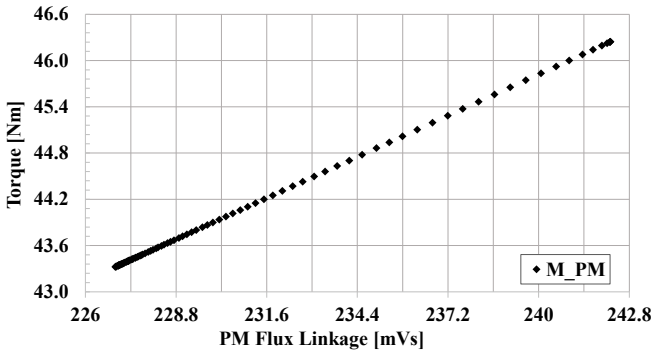

Fig. 20. Derating of the torque production for MUT_2.

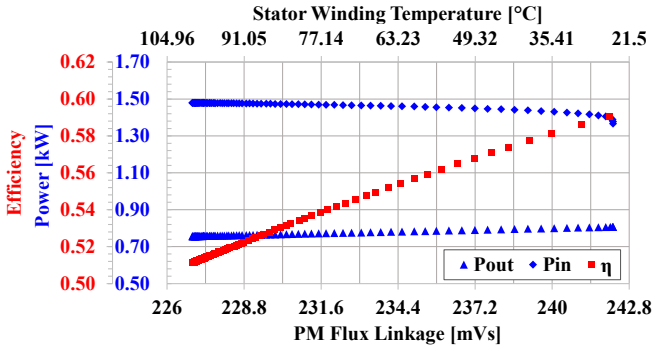

Fig. 21. Expected efficiency of the PM torque production for MUT_2.

MUT_3: The expected results of MUT_3 in terms of PM torque derating are shown in Fig. 22. In this case, the torque derating factor is about k_M = 0.961, thus confirming the temperature-independent behavior of the PM (see Fig. 13). The evolutions of the input and output MUT powers, together with the related efficiency, are shown in Fig. 23. Thanks to the reduced Joule losses, it is noted how the MUT's efficiency is practically constant since it starts from a value of η = 0.936 and decreases to η = 0.923 in steady-state thermal conditions, i.e., corresponding to an efficiency derating factor of $k\eta$ = 0.986.

MUT_4: The expected results of MUT_4 are similar to those obtained on MUT_3, as the decay of the PM flux linkage is negligible (see Fig. 15). The PM torque derating is shown in Fig. 24, thus confirming the excellent value of the torque derating factor, i.e., k_M = 0.972. The evolutions of the input and output MUT powers, together with the related efficiency, are shown in Fig. 25. Like MUT_3, the small value of the Joule losses makes the MUT's efficiency practically constant. Indeed, the latter starts from a value of η = 0.975 and decreases to η = 0.9715 in steady-state thermal conditions, i.e., corresponding to an outstanding efficiency derating factor of $k\eta$ = 0.996.

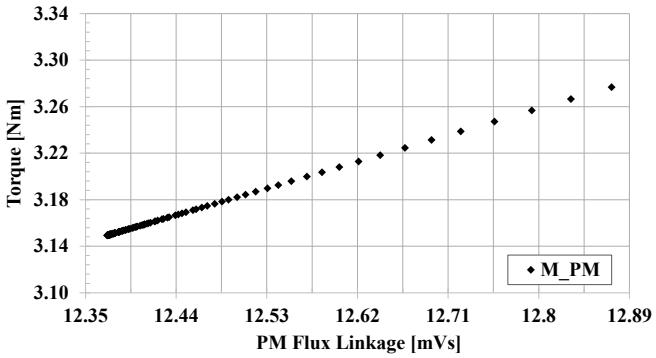

Fig. 22. Derating of the torque production for MUT_3.

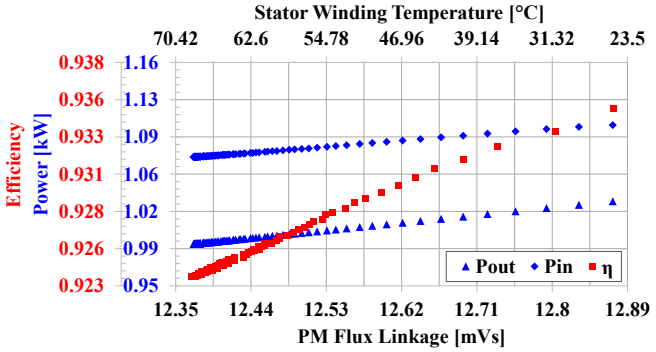

Fig. 23. Expected efficiency of the PM torque production for MUT_3.

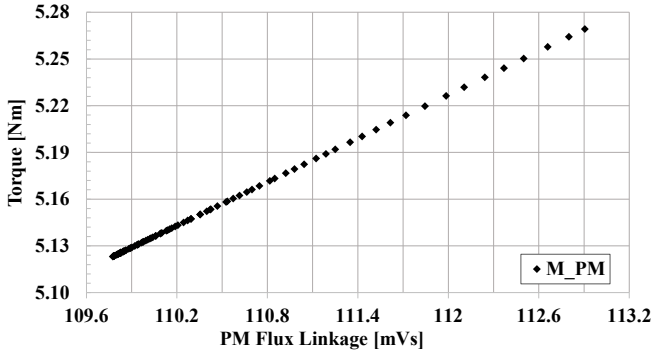

Fig. 24. Derating of the torque production for MUT_4.

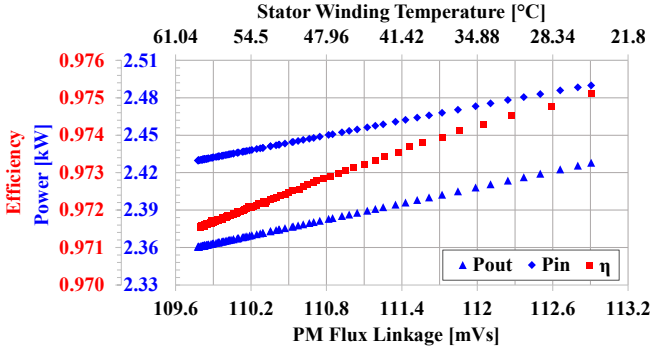

Fig. 25. Expected efficiency of the PM torque production for MUT_4.

TABLE IV. SUMMARY OF THE EXPECTED MUTS PERFORMANCE DUE TO THE PM HEATING

	MUT_1	MUT_2	MUT_3	MUT_4
$M_{PM,0}$	1.78 Nm	46.2 Nm	3.28 Nm	5.27 Nm
$M_{PM,\infty}$	1.34 Nm	43.5 Nm	3.15 Nm	5.12 Nm
k_M	0.753	0.941	0.961	0.972
$P_{j,0}$	78 W	559 W	72 W	62 W
$P_{j,\infty}$	110 W	723 W	82 W	69 W
$\eta_{,0}$	0.88	0.59	0.936	0.975
$\eta_{,\infty}$	0.79	0.51	0.923	0.9715
k_η	0.898	0.864	0.986	0.996

TABLE IV. summarizes the results obtained for the MUTs, showing a potential application of the proposed test procedure.

VIII. CONCLUSION

The paper proposed a novel measurement technique to identify the permanent magnet's (PM) thermal time constant of synchronous ac motors. The proposed test procedure performs the heating of both stator winding and PM by injecting the rated current in the machine under test (MUT). In this way, thanks to a dedicated test rig that uses a calibrated data recorder, the time-evolutions of both stator windings temperature and PM flux linkage during the thermal transient are evaluated. Based on the experimental results, the increment of the PM temperature can be described by a first-order model, so defining a single thermal time constant.

Experimental results for four permanent magnet synchronous machines have been presented, demonstrating the validity of the proposed measurement technique. For MUTs where the design data were available, a comparison between the PM's thermal time constant obtained through the proposed test procedure and the one computed theoretically has been presented, getting the theoretical validation of the proposed methodology, too.

Finally, a preliminary analysis of the derating of MUTs performance due to the PM heating has been reported, demonstrating the effectiveness and a possible application of the proposed measurement technique. Other application examples of the results obtained with the proposed measurement technique concern the definition of robust thermal models directly implemented in parallel with the machine control. In this way, the performance of the torque regulation can be improved, as well as it is possible to implement proper overload strategies of the drive. These aspects consist of the future development of this work.

REFERENCES

[1] 'Ertrac - Welcome'. https://www.ertrac.org/ (accessed 03/2020).

[2] Z. Q. Zhu and D. Howe, 'Electrical Machines and Drives for Electric, Hybrid, and Fuel Cell Vehicles', *Proc. IEEE*, vol. 95, no. 4, pp. 746–765, Apr. 2007, doi: 10.1109/JPROC.2006.892482.

[3] I. Boldea, L. N. Tutelea, L. Parsa, and D. Dorrell, 'Automotive Electric Propulsion Systems With Reduced or No Permanent Magnets: An Overview', *IEEE Trans. Ind. Electron.*, vol. 61, no. 10, pp. 5696–5711, Oct. 2014, doi: 10.1109/TIE.2014.2301754.

[4] G. Pellegrino, A. Vagati, B. Boazzo, and P. Guglielmi, 'Comparison of Induction and PM Synchronous Motor Drives for EV Application Including Design Examples', *IEEE Trans. Ind. Appl.*, vol. 48, no. 6, pp. 2322–2332, Nov. 2012, doi: 10.1109/TIA.2012.2227092.

[5] T. Sebastian, 'Temperature effects on torque production and efficiency of PM motors using NdFeB magnets', *IEEE Trans. Ind. Appl.*, vol. 31, no. 2, pp. 353–357, Mar. 1995, doi: 10.1109/28.370284.

[6] S. Li, D. Han, and B. Sarlioglu, 'Analysis of the influence of temperature variation on performance of flux-switching permanent magnet machines for traction applications', in *2017 IEEE International Electric Machines and Drives Conference (IEMDC)*, May 2017, pp. 1–6, doi: 10.1109/IEMDC.2017.8002084.

[7] A. Boglietti, A. Cavagnino, D. Staton, M. Shanel, M. Mueller, and C. Mejuto, 'Evolution and Modern Approaches for Thermal Analysis of Electrical Machines', *IEEE Trans. Ind. Electron.*, vol. 56, no. 3, pp. 871–882, Mar. 2009, doi: 10.1109/TIE.2008.2011622.

[8] A. Boglietti, A. Cavagnino, and D. Staton, 'Determination of Critical Parameters in Electrical Machine Thermal Models', *IEEE Trans. Ind. Appl.*, vol. 44, no. 4, pp. 1150–1159, Jul. 2008, doi: 10.1109/TIA.2008.926233.

[9] A. M. EL-Refaie, 'Fractional-Slot Concentrated-Windings Synchronous Permanent Magnet Machines: Opportunities and Challenges', *IEEE Trans. Ind. Electron.*, vol. 57, no. 1, pp. 107–121, Jan. 2010, doi: 10.1109/TIE.2009.2030211.

[10] G. D. Demetriades, H. Z. de la Parra, E. Andersson, and H. Olsson, 'A Real-Time Thermal Model of a Permanent-Magnet Synchronous Motor', *IEEE Trans. Power Electron.*, vol. 25, no. 2, pp. 463–474, Feb. 2010, doi: 10.1109/TPEL.2009.2027905.

[11] B. Lee, K. Kim, J. Jung, J. Hong, and Y. Kim, 'Temperature Estimation of IPMSM Using Thermal Equivalent Circuit', *IEEE Trans. Magn.*, vol. 48, no. 11, pp. 2949–2952, Nov. 2012, doi: 10.1109/TMAG.2012.2196503.

[12] A. Boglietti, M. Cossale, S. Vaschetto, and T. Dutra, 'Winding Thermal Model for Short-Time Transient: Experimental Validation in Operative Conditions', *IEEE Trans. Ind. Appl.*, vol. 54, no. 2, pp. 1312–1319, Mar. 2018, doi: 10.1109/TIA.2017.2777920.

[13] A. Boglietti, E. Carpaneto, M. Cossale, and S. Vaschetto, 'Stator-Winding Thermal Models for Short-Time Thermal Transients: Definition and Validation', *IEEE Trans. Ind. Electron.*, vol. 63, no. 5, pp. 2713–2721, May 2016, doi: 10.1109/TIE.2015.2511170.

[14] S. Ayat, H. Liu, F. Chauvicourt, and R. Wrobel, 'Experimental Derivation of Thermal Parameters of the Stator- Winding Region in Thermal Analysis of PM Electrical Machines', in *IECON 2018 - 44th Annual Conference of the IEEE Industrial Electronics Society*, Oct. 2018, pp. 496–501, doi: 10.1109/IECON.2018.8595150.

[15] D. Reigosa, D. Fernandez, T. Tanimoto, T. Kato, and F. Briz, 'Comparative Analysis of BEMF and Pulsating High-Frequency Current Injection Methods for PM Temperature Estimation in PMSMs', *IEEE Trans. Power Electron.*, vol. 32, no. 5, pp. 3691–3699, May 2017, doi: 10.1109/TPEL.2016.2592478.

[16] D. Fernández, M. Martínez, D. Reigosa, A. B. Diez, J. M. Guerrero, and F. Briz, 'Comparative Analysis of Magnet Thermal and Magnetization State Monitoring in PMSMs Based on High-Frequency Signal Injection', *IEEE Trans. Ind. Appl.*, vol. 56, no. 1, pp. 344–357, Jan. 2020, doi: 10.1109/TIA.2019.2952027.

[17] D. Fernandez *et al.*, 'Permanent Magnet Temperature Estimation in PM Synchronous Motors Using Low-Cost Hall Effect Sensors', *IEEE Trans. Ind. Appl.*, vol. 53, no. 5, pp. 4515–4525, Sep. 2017, doi: 10.1109/TIA.2017.2705580.

[18] H. Guo, Q. Ding, Y. Song, H. Tang, L. Wang, and J. Zhao, 'Predicting Temperature of Permanent Magnet Synchronous Motor Based on Deep Neural Network', *Energies*, vol. 13, no. 18, Art. no. 18, Jan. 2020, doi: 10.3390/en13184782.

[19] D. D. Reigosa, D. Fernandez, T. Tanimoto, T. Kato, and F. Briz, 'Permanent-Magnet Temperature Distribution Estimation in Permanent-Magnet Synchronous Machines Using Back Electromotive Force Harmonics', *IEEE Trans. Ind. Appl.*, vol. 52, no. 4, pp. 3093–3103, Jul. 2016, doi: 10.1109/TIA.2016.2536579.

[20] D. D. Reigosa, D. Fernandez, Z. Zhu, and F. Briz, 'PMSM Magnetization State Estimation Based on Stator-Reflected PM Resistance Using High-Frequency Signal Injection', *IEEE Trans. Ind. Appl.*, vol. 51, no. 5, pp. 3800–3810, Sep. 2015, doi: 10.1109/TIA.2015.2437975.

[21] D. Fernández, M. Martínez, D. Reigosa, J. M. Guerrero, C. M. S. Alvarez, and F. Briz, 'Impact of Machine Magnetization State on Permanent Magnet Losses in Permanent Magnet Synchronous Machines', *IEEE Trans. Ind. Appl.*, vol. 55, no. 1, pp. 344–353, Jan. 2019, doi: 10.1109/TIA.2018.2867326.

[22] Z. Q. Zhu, X. Zhu, P. D. Sun, and D. Howe, 'Estimation of Winding Resistance and PM Flux-Linkage in Brushless AC Machines by Reduced-Order Extended Kalman Filter', in *2007 IEEE International Conference on Networking, Sensing and Control*, Apr. 2007, pp. 740–745, doi: 10.1109/ICNSC.2007.372872.

[23] X. Xiao, C. Chen, and M. Zhang, 'Dynamic Permanent Magnet Flux Estimation of Permanent Magnet Synchronous Machines', *IEEE Trans. Appl. Supercond.*, vol. 20, no. 3, pp. 1085–1088, Jun. 2010, doi: 10.1109/TASC.2010.2041435.

[24] K. Liu, Q. Zhang, J. Chen, Z. Q. Zhu, and J. Zhang, 'Online Multiparameter Estimation of Nonsalient-Pole PM Synchronous Machines With Temperature Variation Tracking', *IEEE Trans. Ind. Electron.*, vol. 58, no. 5, pp. 1776–1788, May 2011, doi: 10.1109/TIE.2010.2054055.

[25] H. Kim, H. Jung, S. Sul, and D. J. Berry, 'IPMSM Magnet Temperature Estimation by d-axis Flux Linkage', in *2019 10th International Conference on Power Electronics and ECCE Asia (ICPE 2019 - ECCE Asia)*, May 2019, pp. 2517–2522.

[26] C. Kral, A. Haumer, and S. B. Lee, 'A Practical Thermal Model for the Estimation of Permanent Magnet and Stator Winding Temperatures', *IEEE Trans. Power Electron.*, vol. 29, no. 1, pp. 455–464, Jan. 2014, doi: 10.1109/TPEL.2013.2253128.

[27] M. Ganchev, C. Kral, H. Oberguggenberger, and T. Wolbank, 'Sensorless rotor temperature estimation of permanent magnet synchronous motor', in *IECON 2011 - 37th Annual Conference of the IEEE Industrial Electronics Society*, Nov. 2011, pp. 2018–2023, doi: 10.1109/IECON.2011.6119449.

[28] M. Ganchev, C. Kral, and T. Wolbank, 'Compensation of speed dependency in sensorless rotor temperature estimation for permanent magnet synchronous motor', in *2012 XXth International Conference on Electrical Machines*, Sep. 2012, pp. 1612–1618, doi: 10.1109/ICElMach.2012.6350095.

[29] E. Armando, A. Boglietti, S. Musumeci, S. Rubino, E. Carpaneto, and D. Martinello, 'Measurement Technique for the Permanent Magnet Rotor Thermal Time Constant Determination', in *2020 IEEE International Conference on Industrial Technology (ICIT)*, Feb. 2020, pp. 193–198, doi: 10.1109/ICIT45562.2020.9067271.

[30] E. Armando, A. Boglietti, S. Musumeci, S. Rubino, E. Carpaneto, and D. Martinello, 'Measurement of Rotor Thermal Time-Constant for Permanent Magnet Synchronous Machines', in *2020 IEEE Energy Conversion Congress and Exposition (ECCE)*, Oct. 2020, pp. 4246–4252, doi: 10.1109/ECCE44975.2020.9235959.

[31] P. Krause, O. Wasynczuk, S. D. Sudhoff, and S. Pekarek, *Analysis of Electric Machinery and Drive Systems*. John Wiley & Sons, 2013.

[32] A. Boglietti, R. Bojoi, S. Rubino, and M. Cossale, 'Overload Capability of Multiphase Machines under Normal and Open-Phase Fault Conditions: a Thermal Analysis Approach', *IEEE Trans. Ind. Appl.*, vol. 56, no. 3, pp. 2560–2569, Mar. 2020, doi: 10.1109/TIA.2020.2978767.

[33] E. Armando, P. Guglielmi, G. Pellegrino, and R. Bojoi, 'Flux linkage maps identification of synchronous AC motors under controlled thermal conditions', in *2017 IEEE International Electric Machines and Drives Conference (IEMDC)*, May 2017, pp. 1–8, doi: 10.1109/IEMDC.2017.8002334.

[34] '112-2017 - IEEE Standard Test Procedure for Polyphase Induction Motors and Generators'.

[35] E. Armando, R. I. Bojoi, P. Guglielmi, G. Pellegrino, and M. Pastorelli, 'Experimental Identification of the Magnetic Model of Synchronous Machines', *IEEE Trans. Ind. Appl.*, vol. 49, no. 5, pp. 2116–2125, Sep. 2013, doi: 10.1109/TIA.2013.2258876.

[36] R. Bojoi, E. Armando, M. Pastorelli, and K. Lang, 'Efficiency and loss mapping of AC motors using advanced testing tools', in *2016 XXII International Conference on Electrical Machines (ICEM)*, Sep. 2016, pp. 1043–1049, doi: 10.1109/ICELMACH.2016.7732654.

[37] G. Pellegrino, R. I. Bojoi, P. Guglielmi, and F. Cupertino, 'Accurate Inverter Error Compensation and Related Self-Commissioning Scheme in Sensorless Induction Motor Drives', *IEEE Trans. Ind. Appl.*, vol. 46, no. 5, pp. 1970–1978, Sep. 2010, doi: 10.1109/TIA.2010.2057395.

[38] 'GEN7tA - High Channel Count Data Acquistion System and Tran', *HBM*, Jun. 17, 2020. https://www.hbm.com/en/4674/genesis-highspeed-gen7ta-high-speed-daq/ (accessed Jun. 25, 2020).

[39] A. Boglietti, A. Cavagnino, M. Lazzari, and M. Pastorelli, 'A simplified thermal model for variable-speed self-cooled industrial induction motor', *IEEE Trans. Ind. Appl.*, vol. 39, no. 4, pp. 945–952, Jul. 2003, doi: 10.1109/TIA.2003.814555.

[40] 'Miotti | Components for Electric Motors', *Miotti*. http://www.miottisrl.com/en/ (accessed Nov. 04, 2020).

[41] 'e-Magnets UK | Online Magnet Manufacturer and Supplier', *Bunting - eMagnets*. https://e-magnetsuk.com/ (accessed Nov. 06, 2020).

[42] 'International Standard IEC 60034 - Rotating electrical machines'. [Online]. Available: https://webstore.iec.ch/publication/62415.